Meltback of Hesperian-aged ice-rich deposits near the south pole of Mars: Evidence for drainage channels and lakes

Sarah M. Milkovich, James W. Head III, and Stephen Pratt
Department of Geological Sciences, Brown University, Providence, Rhode Island, USA

Received 17 October 2001; revised 28 December 2001; accepted 3 January 2002; published 27 June 2002.

[1] Mars Orbiter Laser Altimeter (MOLA) topographic data support the presence of an extensive Hesperian-aged volatile-rich south polar deposit, the Dorsa Argentea Formation (DAF) and related deposits, underlying the present Amazonian-aged cap. The eastern margin of these deposits displays further evidence for meltback, ponding, and drainage of the volatile-rich deposit. Channels leading from the margins of the DAF deposit enter nearby craters and are interpreted to represent drainage of water, ice, and sediment from the DAF. Channels connecting these craters provide evidence for extensive crater flooding, ponding (minimum volumes $\sim 10^{12}$ m^3), overtopping, downcutting, and further drainage of material through a series of craters and into the Prometheus Basin near the edge of the current cap. Topography data show that water filled some craters to depths of at least 200 m and possibly as much as 600 m. Materials derived from melting of this lobe of the DAF drained over a lateral distance of $\sim$600 km and a vertical height of $\sim$800 m, partially emptying into the Prometheus Basin. These combined observations imply that meltback of the older, volatile-rich deposit was a widespread event, occurring on both sides of the deposit over a distance of at least 1800 km, and in an area possibly as much as $\sim 2.9 \times 10^6$ km^2. Candidate top-down and bottom-up melting scenarios are examined; the presence of associated Hesperian-aged volcanic deposits and possible subglacial edifices suggests that local and regional basal heating was a major factor in generating the meltwater that formed the drainage features. *INDEX TERMS:* 6225 Planetology: Solar System Objects: Mars; 5416 Planetology: Solid Surface Planets: Glaciation; 5470 Planetology: Solid Surface Planets: Surface materials and properties; 3309 Meteorology and Atmospheric Dynamics: Climatology (1620); 5418 Planetology: Solid Surface Planets: Heat flow; *KEYWORDS:* Mars, polar, glaciers, Hesperian, channels, water

1. Introduction

1.1. Geologic History of the South Polar Region

[2] The general geological history of the south polar region has been outlined by *Tanaka and Scott* [1987] and elaborated upon by *Kolb and Tanaka* [2001] and *Head and Pratt* [2001a] (Figure 1). The earliest units are the cratered terrains of the Noachian, ranging from units associated with the Hellas and Argyre impact basins to heavily cratered plateaus which extend into the Hesperian Period. These are followed by the Dorsa Argentea Formation (Hd; subsequently referred to as the DAF), a topographically low plain composed of broad smooth deposits which embay the older highland units, as well as large irregular pits such as Angusti and Sisyphi Cavi.

[3] Also in this formation are the Dorsa Argentea, a NW-SE trending sinuous ridge system approximately 50–250 km wide and 850 km long. These ridges were interpreted by *Tanaka and Scott* [1987] and others as eolian or lava flow related formations on the basis of Viking images. *Head and Pratt* [2001a] reassessed these features using Mars Orbiter Laser Altimeter (MOLA) topography and concluded that they were very similar to terrestrial eskers, or long, sinuous ridges of sand and gravel which filled drainage tunnels at the base of a glacier as it retreated [e.g., *Benn and Evans*, 1998; *Head and Hallet*, 2001a, 2001b]. The DAF lies at about 1000–1800 m in elevation, predominately lower than Apl, the polar layered terrain. It is areally extensive and asymmetrical about the pole, ranging from 83° to 57°S and 252° to 130°W; this asymmetry is in the opposite direction from that of Apl [*Head*, 2000a]. This formation is interpreted to be a Hesperian-aged volatile-rich deposit [*Head and Pratt*, 2001a].

[4] An associated deposit is HNu, a rough massive deposit found in walls and the floors of cavi (large, irregular pits) and as rounded hills. *Head and Pratt* [2001a] conclude that these cavi are most likely formed by basal melting of a volatile-rich layer. HNu ranges in elevation from less than 500 m to more than 2500 m; it is located largely within the DAF deposits and is considered to be Hesperian in age [*Head and Pratt*, 2001a]. MOLA local and regional topographic data support the presence of these deposits underlying the present Amazonian-aged cap; the DAF and HNu are excellent candidates for ancient polar deposits formed at a cold trap located near the pole [*Head and Pratt*, 2001a]. Combined, they cover an area of 1.52×10^6 km^2, which is slightly larger than the current polar deposits. If these

0148-0227/02/2001JE001802$09.00

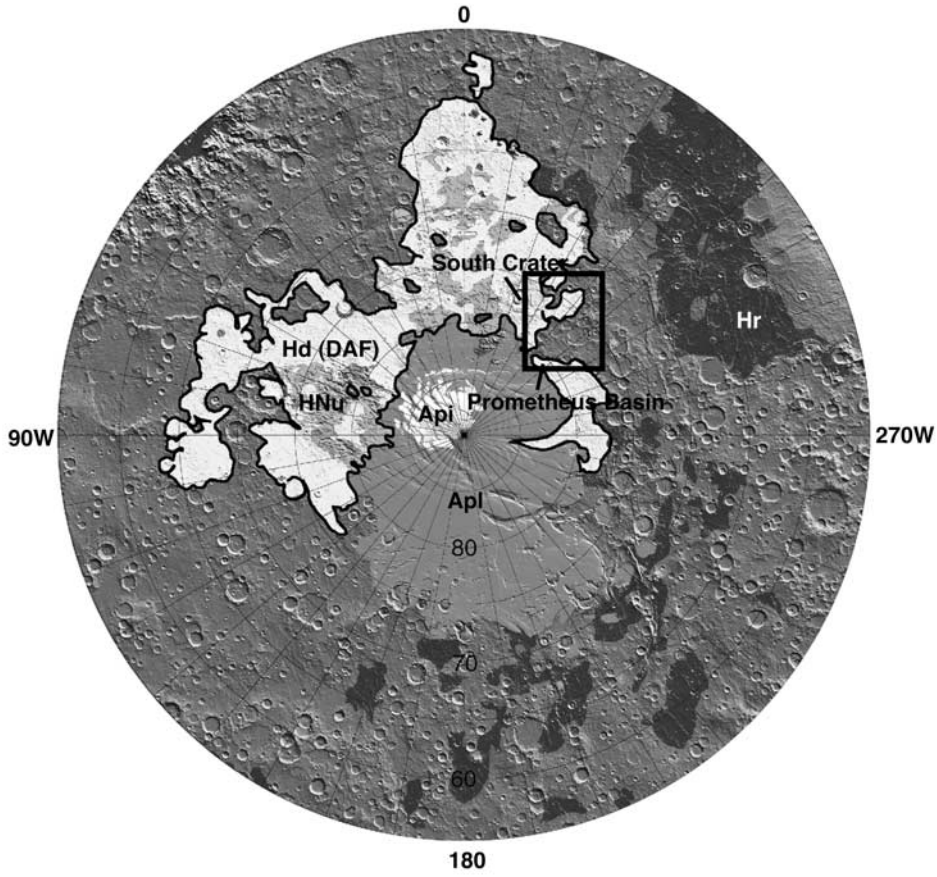

Figure 1. Generalized geologic map of the south polar region [after *Head and Pratt*, 2001a; *Tanaka and Scott*, 1987]; the box in the upper right indicates the location of the region studied in this paper. Geologic units are as follows: Amazonian polar residual ice (Api) is white. Amazonian polar layered terrain (Apl) is medium gray. Hesperian Dorsa Argentea Formation is outlined in black with Hesperian-Noachian undivided (HNu) in light gray. Hesperian ridged volcanic plains (Hr) are dark gray; the rest is the Noachian cratered terrain and plateau sequence. Projection is stereographic.

formations do indeed extend under the present polar deposits, they would cover an area of 2.94×10^6 km^2, or 2% of the surface of Mars [*Head and Pratt*, 2001a]. Formation and modification of these polar-like deposits essentially ended by the middle of the Hesperian [*Plaut et al.*, 1988]; the Hesperian Period began 3.7–3.5 billion years ago and ended 3.3–2.9 billion years ago [*Hartmann and Neukum*, 2001; *Ivanov*, 2001].

[5] A major hiatus occurs in the record between these deposits and the youngest units, the Late Amazonian polar layered deposits (Apl) and the polar ice deposits (Api). Apl is characterized by alternating layers of dark and light material in a smooth, medium albedo material with sparse craters. The base of this deposit is at ~1800 m elevation, and it is asymmetric about the pole (ranging from 70° to 80°S and 140° to 245°W) [*Tanaka and Scott*, 1987]. Api is surrounded by Apl and forms the residual southern cap; it is offset ~200 km north from the pole at 45°W [*Tanaka and Scott*, 1987].

1.2. Previous Studies of the Dorsa Argentea Formation

[6] Several lines of evidence for subglacial melting suggest meltback of the volatile-rich Dorsa Argentea Formation (DAF) in other locations. Previous work by *Head and Pratt* [2001a] documented the existence of four major channels (Figure 2) which emerge from the northwest part of the 0° longitude lobe of these deposits and extend downslope, apparently draining meltwater [*Head and Pratt*, 2001a; *Head*, 2000b]. These four channels are closely associated with the distinctive DAF deposits interpreted to be both volatile-rich [*Tanaka and Scott*, 1987] and of polar origin [*Head and Pratt*, 2001a; *Head*, 2000a]. They begin at the margins of the regional deposit at elevations of ~1000–1500 m and drain downslope 900–1600 km onto the floor of the Argyre Basin, some 3.5–4.0 km below their origin. They do not exhibit minor tributaries, dendritic patterns, or other such features that would suggest runoff from regional precipitation or extensive groundwater sapping over their course. These channels are interpreted to represent distal downslope distribution systems of the meltwater associated with extensive and varied melting within the DAF (e.g., sinuous ridges similar to terrestrial eskers, cavi, chasmata). The broad lateral distribution of these channels (Figure 2) along the margins of the DAF deposit (each separated by 200–400 km lateral distance) supports other evidence [*Head and Pratt*, 2001a; *Head*, 2000a] that basal melting

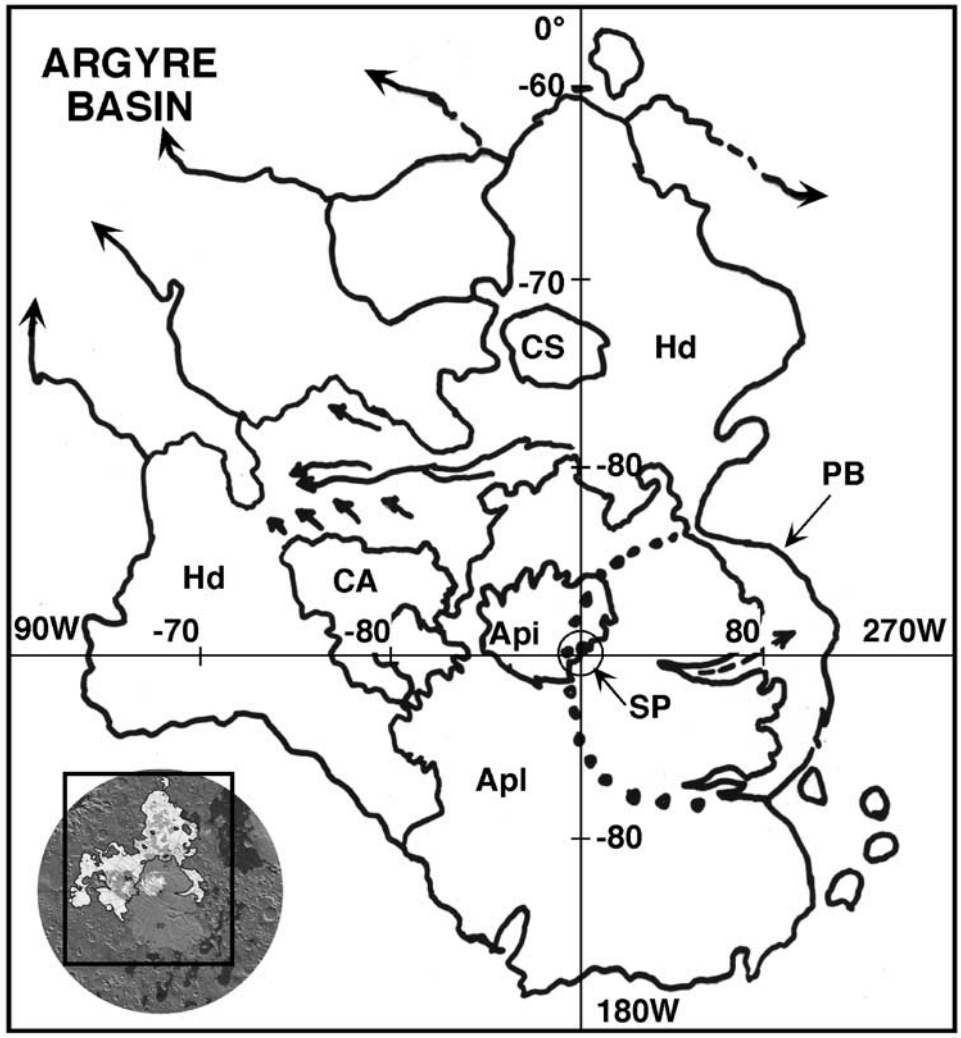

Figure 2. Sketch map showing the location of the channels leading from the western edge of the Dorsa Argentea Formation to the surrounding lowlands and into the Argyre Basin. The distribution of Api, Apl, Hd, and HNu and features associated with the south polar deposits are also shown. SP, south pole; PB, Prometheus Basin; dotted line shows extension under polar cap; dashed line shows Chasma Australe; CA, Cavi Angusti; CS, Cavi Sisyphi; arrows within Hd are Dorsa Argentea esker-like ridges, and arrows outside Hd are channels interpreted to be draining Hd. Inset map shows location of sketch map relative to the geologic map of the south polar region of Figure 1 [after *Head and Pratt*, 2001a].

was areally very widespread and volumetrically significant. Notch-like depressions where the channels cut through preexisting topography in several places along their courses suggest that ponding, overflow, and downcutting may have occurred. Thus some of the unusually flat nature of the intercrater plains may be due to ponding and sedimentation, as well as solidification of ponded water to form ice deposits.

[7] Additional studies by *Head and Pratt* [2001b] examining the fate of this meltwater focus on the region near Schmidt Crater (located along the eastern margin of Cavi Angusti, labeled CA in Figure 2). East of this crater is a north-northwest oriented valley, designated Schmidt Valley, ~350 km wide and over 750 km long. It extends from the edge of the present cap toward the Argyre Basin and is bounded by Noachian cratered terrain on the western, northern, and eastern sides (Figures 1 and 2). The regionally flat floor is at an elevation of ~900–1000 m, while the margins of the valley rise to ~1200–2000 m. The presence of cavi, esker-like ridges, pits, and smooth areas outside Schmidt Valley suggests that the liquid water draining from the melting of the DAF flowed into it. The esker-like features terminate at ~1000 m elevation around the margins of Schmidt Valley, providing evidence that the valley filled with water and became a lake. A notch-like breach in the distal end of the valley and a 400–500 km long channel extending between the notch down into the Argyre Basin suggest that the lake drained into the Argyre Basin.

[8] Further work by *Head and Ghatan* [2001] investigates the interior of the DAF and related units to assess evidence for melting and drainage there. They find that the presently exposed DAF lies within an irregular depression and contains esker-like features, large linear and irregular

depressions such as the Cavi Sisyphi, and meandering channel-like features. The features within this broad depression tend to cluster in regions, and each region is associated with major drainage features at the edge of the DAF. This is consistent with melting in the interior of the DAF.

[9] *Head and Pratt* [2001a] discuss possible causes for this meltback. There are two basic options: from the top down and from the bottom up. Melting from the top down will occur when solar insolation and/or the atmospheric temperature increases. This could happen locally or on a global scale; local temperature increases can be caused by increased insolation due to an extreme obliquity variation or true polar wander, while global temperature increases can be caused by extensive global climate change. Melting from the bottom up can occur through basal melting of a thickened ice sheet or when the broad geothermal gradient increases under the ice sheet. An increased geothermal gradient could lead not only to melting of polar deposits but also to volcanic eruptions. These mechanisms will be discussed further in section 4.2.

1.3. Eastern Margin of the Dorsa Argentea Formation

[10] In order to discriminate between these two melting mechanisms, it is necessary to assess the extent of the melting as well as the relationship of the DAF to other units of similar age which might contain evidence for the cause of meltback. It is therefore important to consider whether the meltback observed on the western margin of the DAF was a local event associated only with the western margin or was much more widespread in the formation.

[11] In this analysis we use MOLA data to examine the margins of DAF on the eastern side of this lobe in an area centered at about 78°S, 310°W (see box in Figures 1 and 3). Two hundred Mars Orbiter Camera (MOC) images in the region 75°–80°S latitude, 200°–230° longitude were also examined. These include all of the images in the area studied that have gone through review and are available on the Planetary Image Atlas Web site; the last of these was taken 17 December, 2000, during orbit 4223. These also include the available images from the most recent releases on the Malin Space Science Systems Web site. We found that the MOC images uniformly provided detailed views of fine-scale surface modification processes (e.g., dunes, frosts, etc.) and did not provide information that was useful to the characterization of the features and relationships at the scale of kilometers to tens of kilometers. We thus relied almost solely on the MOLA data to characterize the surface features at this intermediate scale (Figures 3–7). The area studied is on the opposite side of the DAF from previous studies, some 1800 km to the southeast, far enough away from other signs of meltback and drainage to be able to determine whether or not these events occurred widely.

2. Observations

2.1. Marginal Parts of the Dorsa Argentea Formation

[12] In the region under analysis, the Dorsa Argentea Formation has been mapped in the northern and western part of the area (Figures 3 and 4); in the west it is partially obscured by ejecta from South Crater [*Tanaka and Scott*, 1987]. Figure 5 contains topographic profiles across this region in orthogonal northwest-southeast and northeast-southwest directions. Features in this part of the deposit include the following:

2.1.1. A mantle of debris covering subjacent craters

[13] The upper half of the mapped area generally lacks old craters (Figure 3). Most of the few craters discernible in this region are fresh and young and appear superposed on mantling deposits (see the two central-peaked craters along profile A, Figure 5). The eastern (lower) region has an abundance of craters in various stages of degradation (Figure 4, craters A–G; Figure 5, profiles C, D, H–J). The dashed line in Figure 4 denotes the boundary between high and low crater density and generally corresponds to the eastern edge of the DAF (as mapped by *Tanaka and Scott* [1987]); indeed, many of the craters along this line only retain rims below this line. A portion of the rim of crater A, for example, appears to cut off abruptly at the line. Above the dashed line, the topography is still quite varied; this suggests that the region was not simply covered over and smoothed out by volcanic flooding. Additionally, the sharp boundary in crater density and the lack of flow features and embayed landforms do not support volcanic flooding. Instead, we interpret these characteristics and relations to indicate that the region was blanketed by the DAF.

2.1.2. Depression to the northwest

[14] Toward the upper middle of the mapped region the topography is lower by several hundred meters on average (Figures 3 and 5; compare profiles A and B). This is part of the largest subregion of the DAF identified by *Head and Ghatan* [2001] which is characterized elsewhere by cavi and sinuous channels. It contains the lowest topography of the DAF, with the floor at ~1000–1250 m in elevation and pits as low as 800 m elevation. As discussed in section 1.2, this suggests that products of melting from an extensive interior portion of the DAF drained to the edge of the formation [*Head and Ghatan*, 2001], of which the map area forms part of the eastern margin.

2.1.3. Arcuate ridges

[15] These ridges are found in the DAF near the margins of the deposit (Figure 4, upper middle and upper left); they are convex out from the margins and for the most part extend back into the DAF. They are approximately 50–100 km long and reach elevations of 2000 m, 300–400 m higher than the surrounding plains (Figure 5c, profiles J and K). The ridges nearest the margins are associated with arcuate deposits up to several hundred meters in height and many hundreds of meters wide. These deposits are much rougher than the plains surrounding them. Together, each ridge and deposit forms a landform with a steep cliff on one side and a more gentle slope on the other (Figure 5). This morphology is similar to that of terrestrial lateral, or dump, moraines [*Benn and Evans*, 1998]. These moraines are debris ridges left by a stationary glacier following meltback. They contain clasts and boulders carried within and on top of the glacier, and their size is directly related to the length of time the glacier remained stationary. Such moraines often have steep ice-contact slopes and more gentle slopes on the distal side; however, this may change after retreat of the glacier due to the melting of incorporated ice blocks [e.g., *Benn and Evans*, 1998]. On the basis of the similarity of the arcuate ridges to terrestrial moraines, and

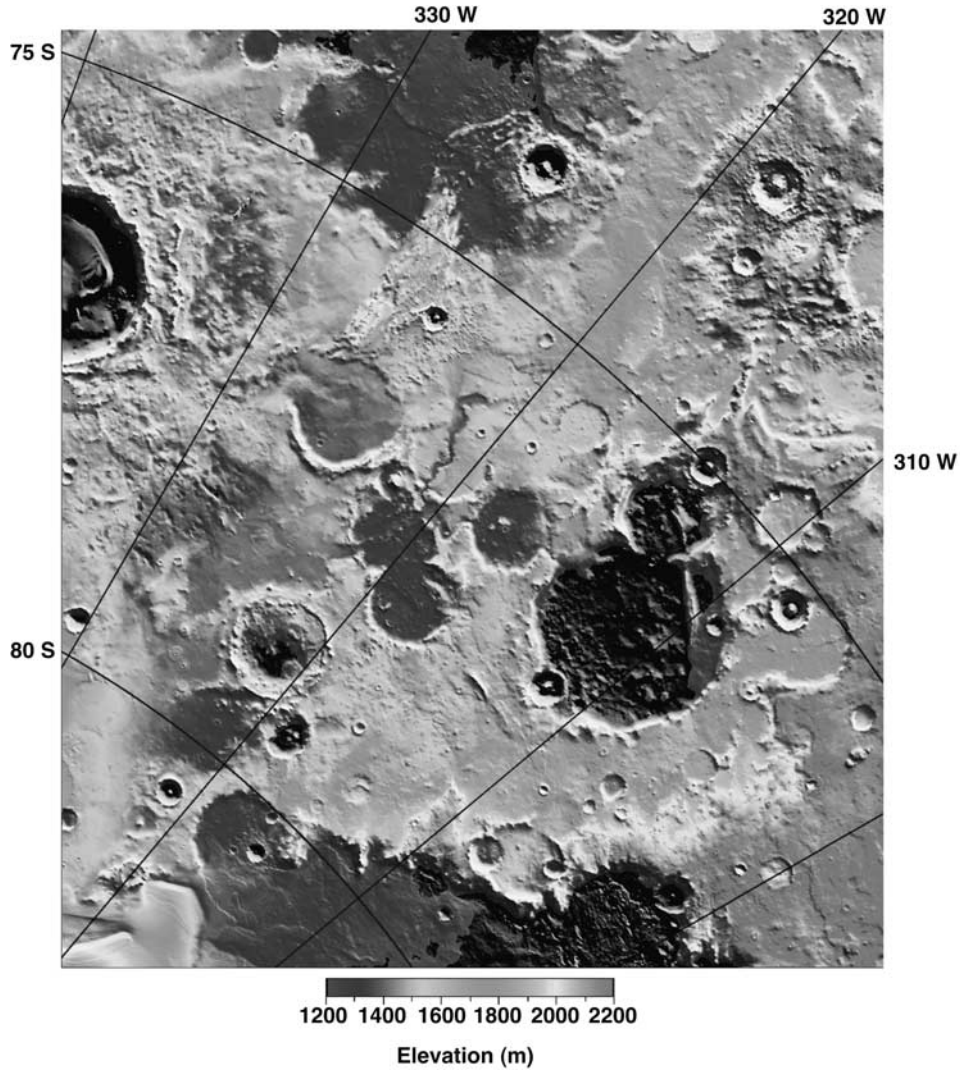

Figure 3. MOLA topography of the south polar region overlain on a topographic gradient map. The gradient map is generated from the same data sets used for topography and consists of directional point-to-point slopes encoded as gray scale. Illumination is from the northeast, and gray is flat, white is upslope, and black is downslope. Projection is stereographic. See color version of this figure at back of this issue.

the range of features suggesting that the DAF was an ancient ice-rich deposit similar to an ice sheet [e.g., *Head and Pratt*, 2001a], we interpret the ridges to be candidates for ancient margins of the DAF.

2.2. Proximal Channels and Craters

[16] At the margin of the DAF (Figures 3 and 4) is a distinctive sinuous channel (channel 1, Figures 4 and 6a) ~2–3 km wide and 30 m deep that extends ~50 km across the plain and through the low part of the rim of crater B, across the crater floor, and down into crater C. The elevation change from the floor of crater B to crater C is ~165 m. A second, less distinct channel (channel 2) emerges from the southwest part of the DAF; its origins are obscured by South Crater ejecta. Channel 2 is straighter and wider than channel 1, although it is still somewhat sinuous. Channel 2 flows for ~70 km across an intercrater plain and enters crater C at a low point in its SSW rim, dropping ~110 m to the crater floor. Both channels lose their identity on the floor of crater C and adjacent crater D.

[17] We interpret these channels to be fluvial and to have been carved from meltwater draining from the margins of the DAF. The relationships described suggest that the products of the channel flow emptied into a closed basin; these products were presumably water and sediment and may have been ice covered or contained ice. The regions adjacent to where the two channels enter crater C tend to be higher (~1315 m) than the lower half of crater D (~1250 m), suggesting that if the two craters had originally similar floor elevations, then sediment approximately 50–60 m thick may have been deposited when the channels entered craters C and D. Another channel, 3, is observed along the northeastern margin of crater C; it is a sinuous structure ~2 km wide connecting crater C with crater E. The floor of crater E lies at an elevation of ~1320 m, about the same as the floors of craters C and D. Another channel,

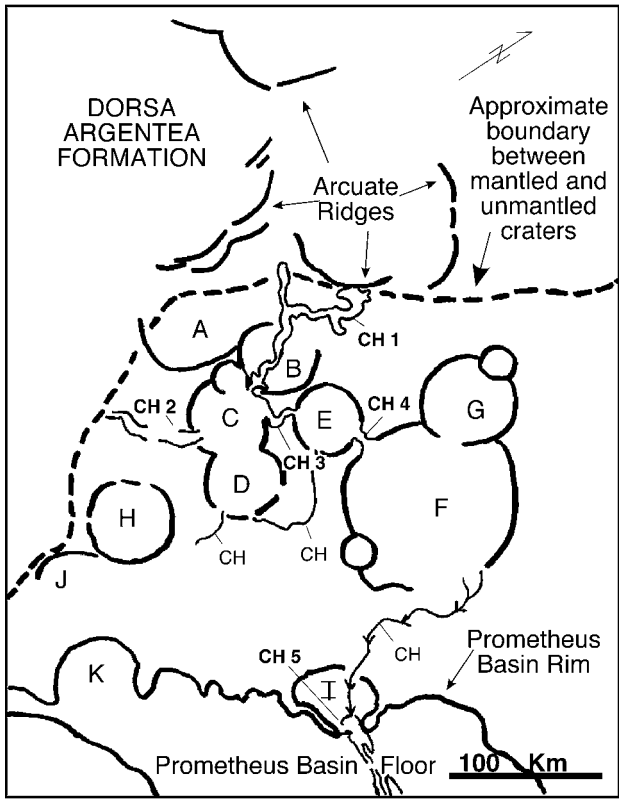

Figure 4. Sketch map of the region studied (Figure 3). Craters are labeled A through K; channels (CH) are numbered 1 through 5. Dashed line shows approximate boundary between mantled and unmantled craters and is equivalent to the margin of the Dorsa Argentea Formation.

channel 4, is observed along the eastern rim of crater E. Channel 4 is straight and narrow and connects crater E and crater F. A topographic profile along the floor of these channels is shown in Figure 6b, and profiles of the widths of these channels are shown in Figure 6c. The floors of crater F (∼910 m) and adjacent crater G (∼950 m) are considerably lower than the floors of the other craters (Figure 5b, profile D; Figure 5c, profile I); crater F is the lowest point in this region (Figures 5b and 5c, profiles D, H, I). On the basis of comparisons with fresh craters on Mars [*Strom et al.*, 1992], these craters appear significantly degraded. They have flat floors, no central peaks, and no recognizable ejecta deposits. Their rims show signs of erosion; for example, the rim of crater D ranges widely from 1500 to 2100 m in elevation (Figures 3 and 5, profiles D and J). Indeed, there is no rim separating it from crater C. In many places the rim of crater D is indistinguishable topographically from the surrounding intercrater plains. This is in sharp contrast to fresh craters, the majority of which have well-defined rims, central peaks, and ejecta deposits [*Strom et al.*, 1992].

2.3. Other Craters and Depressions

[18] An extremely large ancient impact crater appears to underlie the DAF and is partially obscured by the superposed South Crater. Evidence for this ancient crater is the set of arcuate degraded massifs that form a ring ∼200 km in diameter. A portion of these massifs can be seen in the upper left of Figure 3. Crater A (Figure 4), just outside this ancient crater, is very asymmetrical; its southeastern rim is distinctive, while its opposite rim is partly buried and obscured by remnants of the DAF. An extensive plateau extends for several hundred kilometers between craters C, D, E, and F and the Prometheus Basin rim (green and light blue in Figure 3). Low points in the eastern rims of craters F and D suggest that if these craters were filled with water (a depth of ∼580 m), then drainage could have occurred from these craters though low points in their rims into the adjacent shallow intercrater areas. Evidence for this is a series of small channels located in these regions (Figures 3 and 4) and marked CH. Structures on the rim of crater I provide supporting evidence for such activity. In this crater, located at the southeastern margin of the intercrater plains, there is a breach in the northwestern rim of the crater (∼1600 m elevation), and a major channel-like feature cuts the eastern rim. This channel (channel 5, Figure 4) empties out into the floor of the Prometheus Basin, ∼650 m below the intercrater plateau. Additional low points in the Prometheus rim occur just southeast of crater H; here an ancient crater (J) and a younger crater (K) superposed on the Prometheus Basin rim are low relative to the rest of the rim. Ponded meltwater could have exited through this low, although no evidence for channels is observed there. Linear and arcuate ridges are observed on the NNE parts of the floors of craters D, F, and G (Figures 3 and 5b, profile D). We speculate that these features may be remnants of the frozen and now largely sublimated deposits that once occupied these craters. Their present location and preservation would be favored by the fact that they are consistently found on the sides of the crater that receive less solar insolation.

3. Flow Evolution

[19] The features, observations, and topographic relationships described above are consistent with earlier interpretations that suggest that the Dorsa Argentea Formation was a previously more extensive volatile-rich ice sheet like deposit [*Head and Pratt*, 2001a; *Head*, 2000a]. Meltback of the DAF produced channels at the margins of the deposit in several areas [*Head and Pratt*, 2001a; *Head*, 2000b], draining material into surrounding regions. In the area examined in this analysis (Figure 3), melt products appear to have emerged from two major points along the edge of the deposit (channels 1 and 2, Figures 4–6). At the northernmost point, water may have ponded between the distal lobes (arcuate convex outward features) and the convex outward southeastern rims of craters A and B. The following three lines of evidence suggest that this ponded water breached the southeastern rim of crater B, causing drainage into craters C, D, E, and F as well as elsewhere downslope:

1. The southern rim of crater B is marked by a deep incision and two short flanking troughs at the edge of the crater floor at the point of exit of channel 1 (Figure 6). In addition, channel 1 is among the widest of the channels observed (Figure 6). We interpret this to mean that meltwater initially flooded crater B and filled it up to a low point in the rim. Upon reaching this low point, the water began to drain out of the crater and rapidly downcut a channel into the rim. Once the downcutting reached the crater floor, erosion of the floor began and was accentuated near the exit point. This

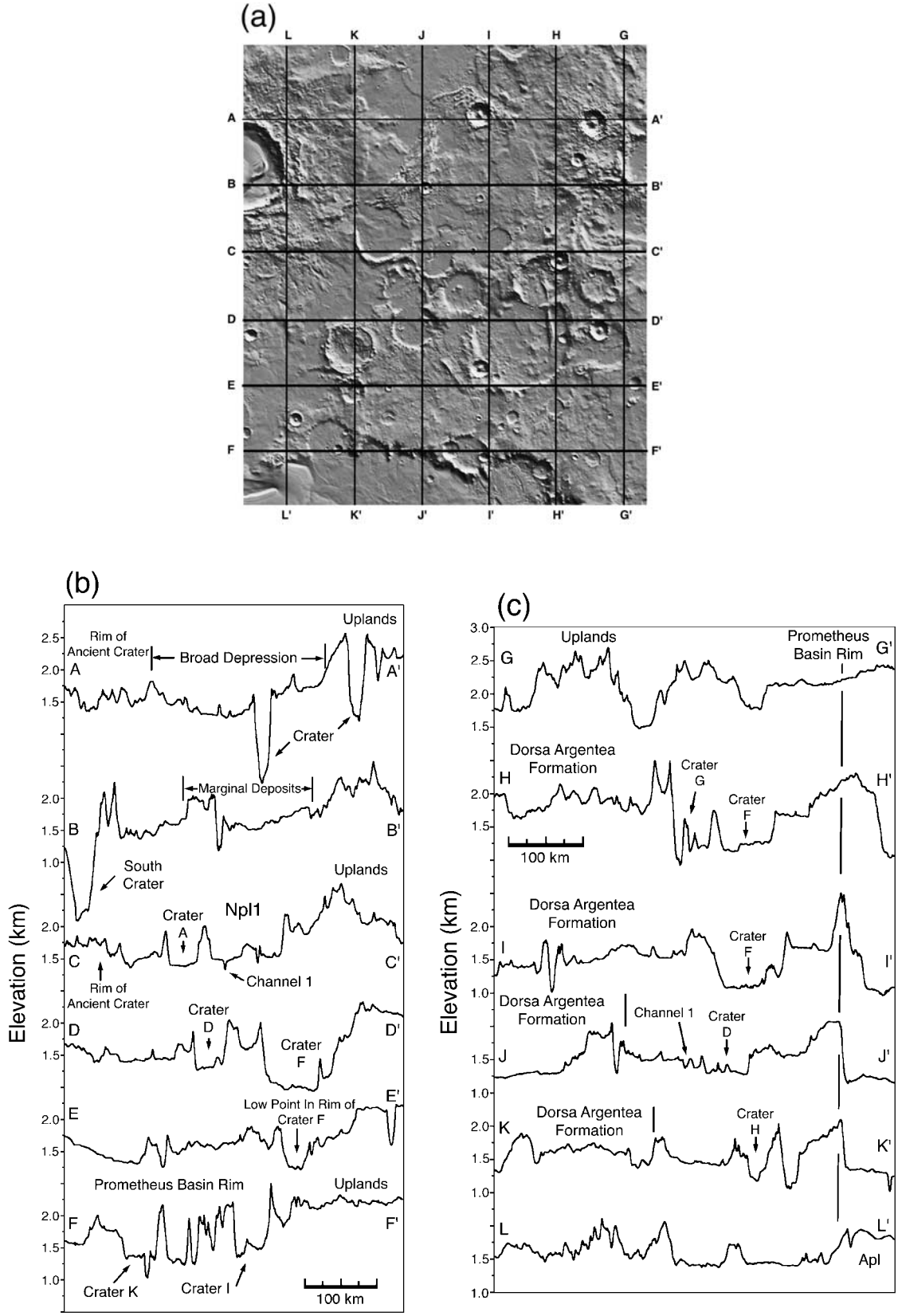

Figure 5. Topography of the eastern region of the Dorsa Argentea Formation. Profiles A–A′ through F–F′ are northeast-southwest across the region, while profiles G–G′ through L-L′ are northwest-southeast across the region studied. (a) Gradient map of region and locations of topographic profiles. (b) Topographic profiles northeast-southwest across region. (c) Topographic profiles northwest-southeast across region.

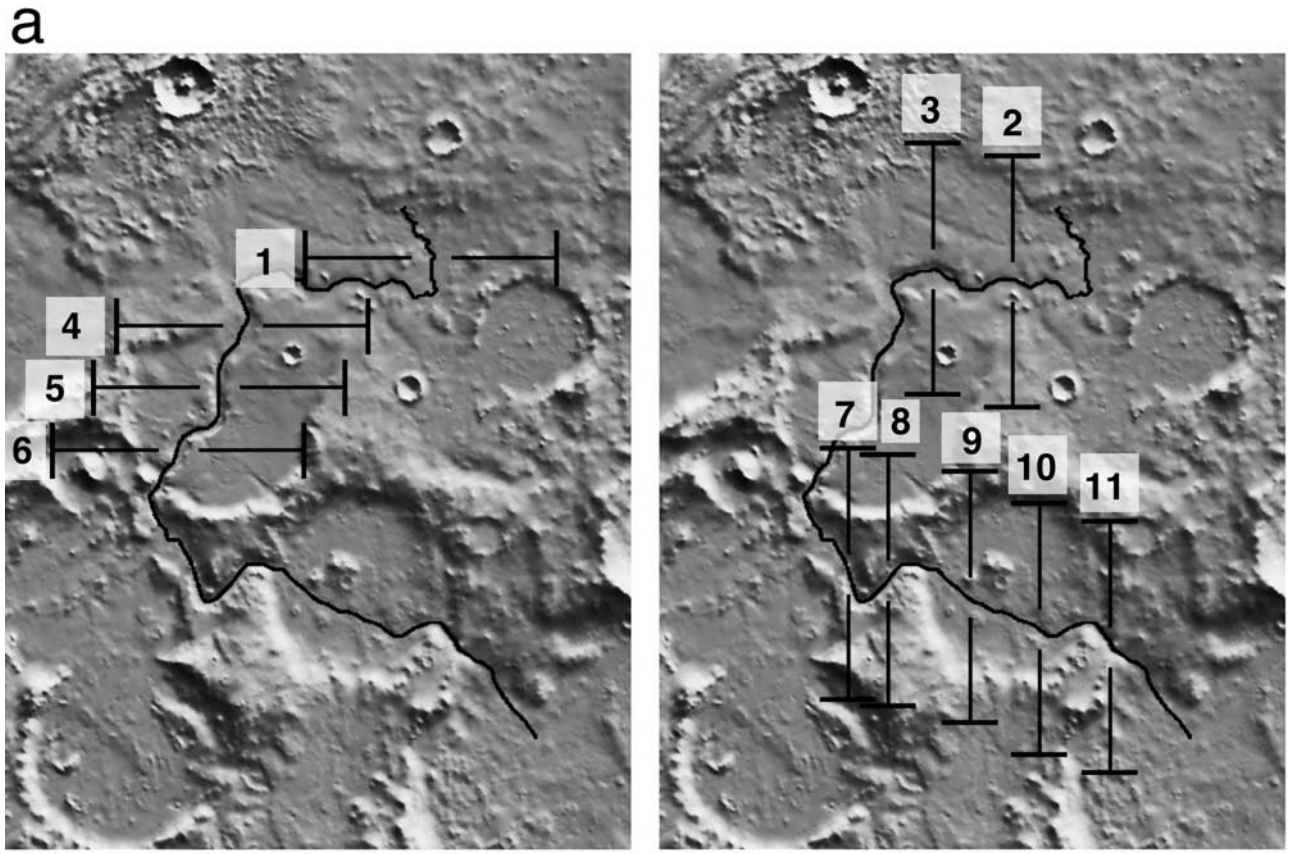

Figure 6. Topography of channels 1–4 in the eastern region of the Dorsa Argentea Formation. These channels connect craters B, C, D, E, and F. Profiles 1 through 6 are from channel 1; profiles 7 and 8 are from channel 3; profiles 9 and 10 are from the floor of crater E; and profile 11 is from channel 4. (a) MOLA topographic data of channels and locations of topographic profiles. (b) Topographic profile along channels connecting craters B, C, D, E, and F. Crater F is at the right-hand side, and crater E is the depression containing profiles 9 and 10. Some of the vertical changes in elevation appear to be related to downslope movement and filling subsequent to the formation of the channels. For example, the topographic highs at profiles 8 and 11 are at crater rims which are the locations of steep-sided incisions in crater walls (see profiles in Figure 6c). All points lie below the initial elevation of the profile at the left; the line represents the 1500 m elevation. (c) Topographic profiles across channels. Arrows point to the channel floors.

formed the two short flanking troughs and began the erosion of the channel back across the crater floor as the flow adapted to the new base level. Subsequently, meltwater draining from the DAF utilized this newly formed channel, widening it in the process. If this interpretation is correct, it suggests that there was a sufficiently deep pond of liquid water for a long enough period of time to downcut and erode the channel. Similar morphologies are observed on Earth when natural dams are breached, for instance in the Channeled Scablands of the American Northwest formed by the breaching of glacial Lake Missoula [e.g., *Baker et al.*, 1987; *Benn and Evans*, 1998].

2. Channel 1 is lower than the rest of the crater floor and wider in this area than most other channels in the region (Figure 6). Figure 6b traces topographic profiles across this channel in locations indicated in Figure 6a; profiles 1 through 6 are from channel 1 and are wider than the majority of the remaining profiles. The widened nature of the channel across the crater floor and the depth of the channel suggest that rapid flow scoured out a deeper, wider path. This incision would have occurred during and after rim breaching and drainage, as described above. Again, this is similar to features seen in glacial Lake Missoula [*Baker et al.*, 1987; *Benn and Evans*, 1998].

3. Channels 1 and 2 have no obvious source point. There are many small channel-like features near the margin of the DAF and many topographically smooth areas that may reflect the former presence of ponded material near the beginnings of the channels (Figure 3). The diffuse nature of the upper reaches of the channels suggests collection of water from a broad local area, perhaps indicative of drainage of ponded water.

[20] In summary, we propose the following sequence of the events in crater B. First, meltwater from the DAF drained to the margins of the deposit and flooded crater B. As meltwater continued to collect, it overtopped the crater,

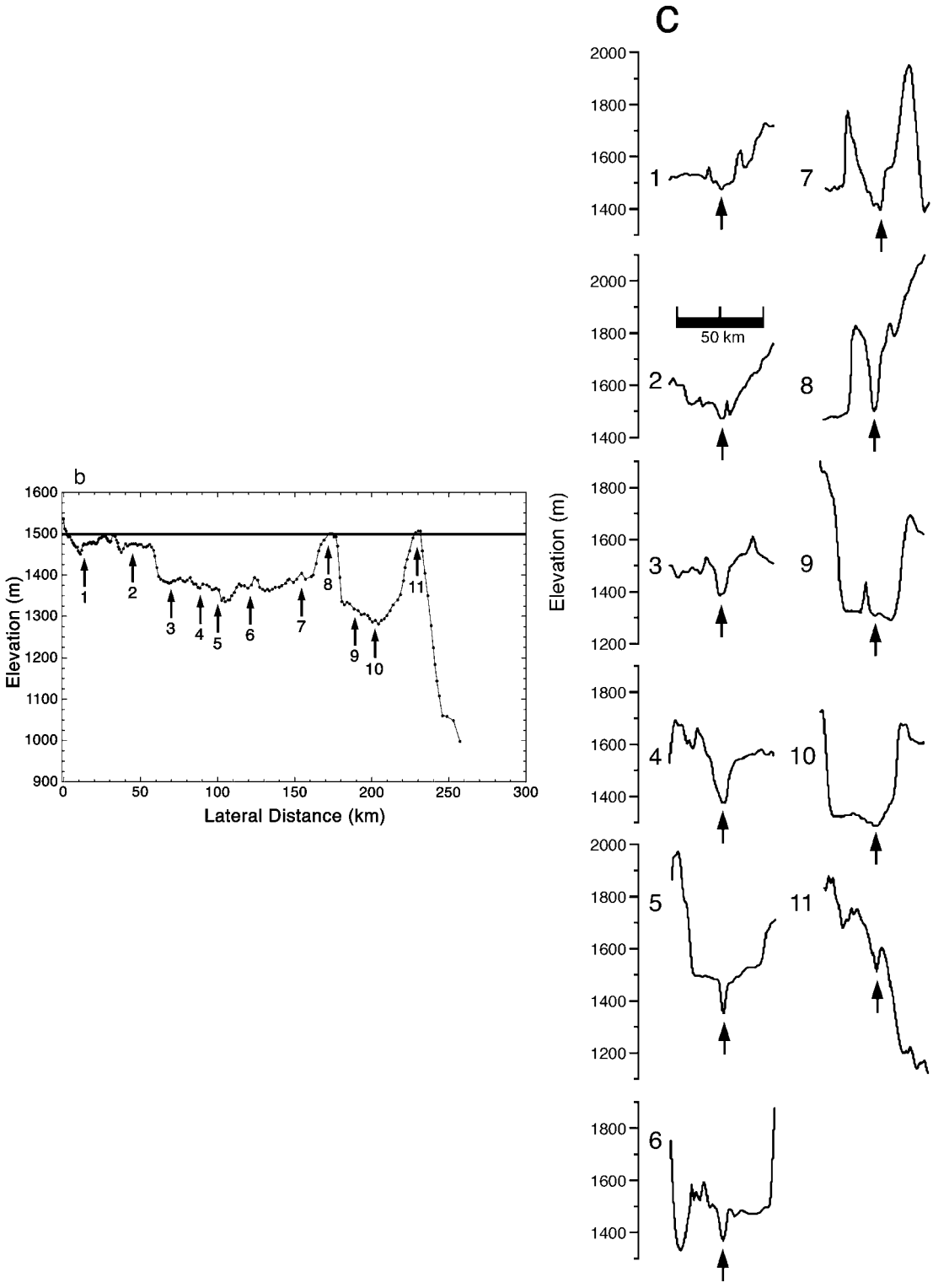

Figure 6. (continued)

flowing over the rim and into crater C. The breaching of the crater rim by the water caused erosion and downcutting to the level of the crater floor. The continuing flow of meltwater eroded the channel back across the floor of crater B a new base level, and drainage continued through this channel.

[21] Once the rim of crater B had been breached, meltwater drained onto the floor of craters C and D and deposited sediment. These craters filled with meltwater to sufficient depths (at least 200 m) that water began to flow through a low in the northeastern rim of crater C. This

incised channel 3 into the rim; water then drained into crater E. Some flow may have exited the southeastern corner of crater E into the adjacent intercrater plains and possibly drained back into crater D (see Figures 3 and 4). After filling crater E, meltwater exited through a low in the eastern rim of the crater onto the floors of crater F and parts of G. Additionally, some flow may have exited the southeastern corner of crater D into the adjacent intercrater plains (see Figures 3 and 4). There is evidence that meltwater then filled crater F (~600 m deep) and flowed out from the eastern margins of the crater rim onto adjacent intercrater areas (see Figures 3 and 4). The southern rim of crater F is lower than the surrounding plains in several locations. A large breach in the northern rim of crater I implies that a significant amount of water flowed into this crater. This suggests that water traveled from crater F across the intercrater plains and into crater I. Water then flowed out through channel 5 in the eastern rim of crater I and onto the Prometheus Basin floor. The most probable path of flow from crater F to crater I is shown by a subtle depression (Figure 3) and is indicated by a line with arrows in Figure 4.

4. Summary and Discussion

4.1. History of the Eastern Dorsa Argentea Formation

[22] An examination of the eastern margins of the Dorsa Argentea Formation, an Hesperian-aged, ice-rich deposit, reveals sinuous channels leading away from the margins and forming interconnections between a series of craters. Topographic data show that these channels served as conduits for water draining from the margins of the DAF as it melted back. As water filled craters and topographic lows at the margin of the deposit, new spillways and channels were formed at low points in the rims. Water filled the adjacent lows, downcutting the channels in the process. As proximal crater rims were breached, channels often cut down and back toward new base levels. Material carried away from the margins of the DAF by channels 1 and 2 traveled through craters B, C, E, F, and I. Along the way some water apparently spilled over into the intercrater plains through low points in the rim of crater D. Water ponded in these craters and may have frozen and sublimated in many of them. For instance, crater C has inflow channels (channels 1 and 2) that are approximately the same depth as the crater floor at their mouth. However, the outflow channels identified on the rims of crater D and F are not as deep as the craters; water entering the depression would fill to the crater rim and then drain out the channel through the low point in the rim. Thus there would always be ~250 m of standing water or ice in the crater during the drainage period.

[23] The water interpreted to have formed these features is no longer there; this implies that it was removed either through freezing and sublimation processes or by soaking into the regolith and the cryosphere [*Clifford*, 1993]. If the environmental conditions at this time were similar to the conditions that exist on the surface of Mars today (average polar surface temperature 154 K, average surface pressure 6.1 mbar [*Clifford*, 1993]), then freezing and sublimation could have happened during or shortly after the meltback of the DAF. If this occurred during a warmer, wetter early Mars, then the water may have ponded in the craters and evaporated or remained until the environment evolved into its current state. Once current conditions were reached, the water would have frozen and sublimated. Standing bodies of water under current conditions would freeze solid and sublimate in geologically very short periods of time unless protected by an insulating layer of debris [e.g., *Carr*, 1996; *Kreslavsky and Head*, 2001]. Topography data show that water filled some craters to depths of at least 200 m (crater C) and possibly as much as 600 m (crater F). Water derived from this lobe of the DAF drained over a distance of at least 600 km and partly emptied into the Prometheus Basin [*Fishbaugh et al.*, 2000], dropping a net vertical distance of 800 m.

4.2. Implications for the Dorsa Argentea Formation and Surrounding Regions

[24] On the basis of our analysis we conclude that the melting of the DAF was not a local event. Evidence for drainage of material from the DAF has been found on both the eastern and western margins of the deposit [*Head and Pratt*, 2001a]. These two margins are separated by a distance of at least 1800 km, and the DAF itself may cover an area of as much as $\sim 2.9 \times 10^6$ km^2. This widespread meltback of a large deposit implies a change in the immediately surrounding environment. Possible causes, briefly discussed in section 1.2, can be divided into top-down mechanisms (e.g., extreme obliquity and/or eccentricity, true polar wander, or global climate change) and bottom-up mechanisms (e.g., basal melting and/or an enhanced local geothermal gradient). Here we assess the impact of, and evidence for, each mechanism.

4.2.1. Top-down mechanisms

[25] Obliquity variations are thought to influence the formation of polar deposits such as the layered terrain presently found at the north and south poles [*Thomas et al.*, 1992]. Extreme obliquity, for example, 60° [*Ward*, 1992], would allow increased insolation to reach the DAF and thus raise the atmospheric temperature at the poles. However, simply increasing the temperature of ice while keeping atmospheric conditions the same will not yield stable liquid water; the atmosphere is relatively dry, and the water would quickly evaporate. Enough water would have to evaporate to raise the water vapor partial pressure to ~10 mbar, 10^4 times greater than the current water content of the atmosphere [e.g., *Jakosky and Phillips*, 2001], before liquid water would be stable at the surface. Furthermore, the cyclical nature of these obliquity variations implies that large-scale deposition and meltback events would have happened many times over the course of Martian history. No evidence for such numerous events has been reported in the geological maps and history of Mars [e.g., *Tanaka et al.*, 1992]; this suggests that either the meltback of the DAF was the last event of this nature or that an extreme obliquity variation was not the sole cause of the meltback of the DAF.

[26] The same logic holds true for the effects of true polar wander [e.g., *Schultz and Lutz*, 1988] on the ice-rich deposits. While true polar wander might reposition the DAF to a location where it would receive increased insolation and therefore higher atmospheric temperatures, increased surface pressure is required to create liquid water. While a change in pressure may have occurred from the rapid sublimation of polar deposits, the current location of

the DAF reduces the likelihood of this event, causing meltback of the DAF. The polar regions are cold traps for water, and thus water naturally collects at the poles [*Clifford*, 1993], and the current location of the DAF is the most probable location for its formation. This suggests that there would have to have been two events of true polar wander, one to move the DAF to a suitable location for melting and one to return it to the southern polar region. The small probability of this occurring causes us to conclude that true polar wander is not a leading candidate for causing the meltback of the DAF. Additionally, studies of surface features and predicted lithospheric stress fields due to polar wander led *Grimm and Solomon* [1986] to conclude that either no substantial polar wander occurred or it occurred before the emplacement of most surface units, and therefore before the formation of the DAF.

[27] *Fishbaugh and Head* [2001] point out that there is evidence that both polar caps were once more extensive and more symmetric about the poles. The DAF in the south and the Olympia Planitia and remnant polar material in the north are possible former portions of the ice caps, and both have undergone melting and retreat. However, the nature and exact timing of these retreats are still unknown. Additionally, there is an extremely long hiatus in the geological record at both poles between the Late Hesperian and the Late Amazonian. *Fishbaugh and Head* [2001] suggest several scenarios to explain this similarity in the north and the south; one possibility is that the polar caps are oscillating with the extremes in the obliquity cycle. At extreme obliquity ($\sim 60^\circ$ [*Ward*, 1992]) the caps sublime and disappear but reform during other parts of the obliquity cycle; such obliquity extremes may have caused the hiatus. However, it is unlikely to have caused the meltwater that flowed through this portion of the margins of the DAF.

[28] Global climate change is a more plausible cause of atmospheric heating; a ''warm, wet early Mars'' could mean increased atmospheric temperatures and increased surface pressure due to a thicker atmosphere. Extensive modeling of the conditions necessary to raise the average global surface temperature to 273 K calls for atmospheres of 0.2–10 bars, depending on which greenhouse gases are invoked, the amount of water available, and the presence and opacity of CO_2 clouds [*Haberle*, 1998]. It is probable that early Mars possessed a thick atmosphere which was later lost by large impacts and solar wind stripping; these loss processes occurred during the late Noachian and early Hesperian Periods [*Jakosky and Phillips*, 2001]. If the warmer conditions persisted into the middle Hesperian, widespread melting and drainage of the DAF would have occurred and the deposit would have lost a significant part of its thickness. However, the DAF has been interpreted to have formed in the middle of the Hesperian [*Tanaka and Scott*, 1987; *Plaut et al.*, 1988]; it is unlikely that such early climate conditions extended that far toward the present. Analysis of Pathfinder data led to estimates of erosion rates through time and the conclusion that erosion rates in the Hesperian were lower by 3–5 orders of magnitude than those in the Noachian, while the Amazonian erosion rates are lower still [*Golombek and Bridges*, 2000]. This suggests that the current climate extends back to the beginning of the Hesperian, 3.5–3.8 Ga. Therefore the DAF appears to have formed after significant climate change had already occurred. A specific phase of extensive volcanism could, however, provide a pulse-like input of volatiles into the atmosphere (e.g., early Hesperian ridged plains, Hr [see *Head et al.*, 2002]).

[29] Temporary climate excursions could provide the conditions necessary for melting. *Baker et al.* [1991] proposed that volcanic eruptions at the Tharsis complex could melt goundwater, causing cataclysmic outflow and ocean formation, and place several bars of CO_2 into the atmosphere [*Baker*, 2001]. The increased CO_2 content of the atmosphere would lead to brief periods of CO_2 greenhouse warming. While modeling of the effects of such a greenhouse demonstrates that 2 bars of CO_2 added to the atmosphere do not allow the polar regions to reach the melting temperature of water, it does suggest that a substantial amount of water may be transported from a frozen body of water, such as a frozen ocean, to high elevations and latitudes [*Gulick et al.*, 1997]. Water deposited as snow on the surface of the DAF could increase the thickness of the deposit and produce basal melting or could act in concert with basal heating, as discussed below.

4.2.2. Bottom-up mechanisms

[30] Basal melting of a volatile-rich deposit occurs when a sufficient additional thickness of material has built up on the surface to cause upward migration of geotherms, resulting in the base of the volatile-rich sheet reaching the melting point. For previous estimates of the current Martian geothermal heat flux of ~ 30 mW m^{-2}, the thickness of deposit required before basal melting begins is 3.3–11.9 km, while for a flux of 90 mW m^{-2} the thickness is 1.1–4 km. These values depend on such factors as dust-ice mixing ratios and the presence of salts [*Clifford*, 1993]. Recent MGS data suggest that the surface heat flow was likely between 20 and 60 mW m^{-2} during the Hesperian [*Zuber et al.*, 2000]. *Head and Pratt* [2001b] estimate that the DAF could have reached thicknesses of 1–3 km. Depending on the dust content of the deposit, basal melting could have occurred if both the thickness and the heat flow were at high values. If the deposit contained CO_2 and clathrates, melting conditions and fluid generation conditions would change accordingly [e.g., *Longhi*, 2000; *Hoffman*, 2000].

[31] Another method of changing the local geothermal gradient is through local advective transport of heat by intrusion or eruption of lavas at the base of a glacier or ice-rich deposit [e.g., *Gudmundsson et al.*, 1997; *Wilson and Head*, 2002]. Ascent and intrusion of magma as dikes and sills into overlying ice transport heat rapidly and efficiently; at typical dike propagation speeds, ice behaves as a brittle solid, which causes dikes to intrude 20–30% into the ice before significant melting begins. The dike therefore provides a large surface area in contact with the ice to allow heat transfer [e.g., *Wilson and Head*, 2002]. This generates large volumes of meltwater which can be released catastrophically at the margins of the ice sheets; such floods are extensive and ongoing in Iceland and are termed jökulhlaups [*Björnsson*, 1992]. This process of interaction of magma and ice-rich material has been documented at several times in the history of Mars (e.g., see review by *Head and Wilson* [2002]) [*Chapman et al.*, 2000; *Ghatan and Head*, 2001, 2002].

[32] Documentation of volcanic activity occurring at the same time as the meltback of the DAF would provide evidence for such an enhanced geothermal phase. Refer-

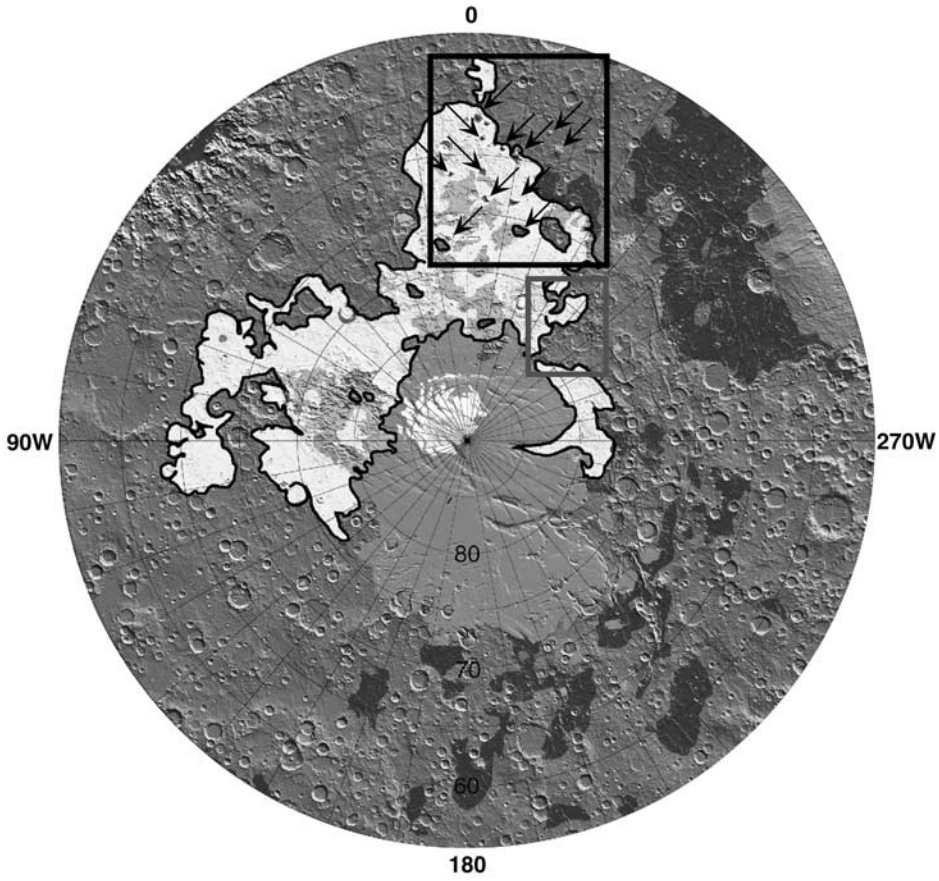

Figure 7. Location of candidate subglacial volcanoes (arrows) in and near the Dorsa Argentea Formation. Black box indicates region where volcanoes were identified by *Ghatan and Head* [2002]; gray box indicates region studied in this paper. Subglacial heating associated with this volcanic activity may have caused the observed melting.

ence to the correlation charts of the 1:15M-scale maps of Mars [e.g., *Greeley and Guest*, 1987; *Scott and Tanaka*, 1986; *Tanaka and Scott*, 1987] shows that the globally extensive ridged plains unit (Hr) of Early Hesperian age overlaps in time the Dorsa Argentea Formation. Similarly, in the south polar region the Amphitrites Formation (Hap, Had) and the upper part of the plateau sequence (Hpl_3), all of candidate volcanic origin, also overlap in time with the DAF. In addition, recent examination of neighboring terrain (Figure 7) has revealed mountains in the DAF which are interpreted to be volcanoes [*Ghatan and Head*, 2001, 2002]. These mountains share many morphological characteristics with Icelandic volcanoes formed under ice sheets; *Ghatan and Head* [2001, 2002] have interpreted them to have formed under the DAF when it was more widespread. In summary, the geothermal heating associated with these widespread units of suspected volcanic origin (Hr, Hap, Had, Hpl_3), and the volcanic complexes and edifices suspected to be of subglacial origin, could have produced widespread melting and drainage of the extensive DAF. In addition, rapid water release is a common consequence in subglacial volcanoes on Earth [*Björnsson*, 1992].

[33] In summary, of the possible causes for the extensive melting of the Dorsa Argentea Formation in the Hesperian, we conclude that the widespread occurrence of volcanism, and the implied local and regional change in geothermal gradient, is a primary candidate. Global climate change may have also played a role but is more difficult to establish.

[34] **Acknowledgments.** Thanks are extended to the Mars Global Surveyor spacecraft and operations teams at the Jet Propulsion Laboratory and Lockheed-Martin Astronautics for providing the engineering foundation that enabled this analysis. Thanks are also extended to the MOLA team for productive discussions and to Greg Neumann for superior professional performance and timely data processing and presentation. We gratefully acknowledge financial support from the NASA Mars Data Analysis Program (grants NAG5-10573 and NAG5-9780) to J.W.H. and from the Brown University Fellowship program to S.M.M.

References

Baker, V. R., Water and the Martian landscape, *Nature*, *412*, 228–236, 2001.

Baker, V. R., R. Greeley, P. D. Komar, D. A. Swanson, and R. B. Waitt, Columbia and Snake River Plains, in *Geomorphic Systems of North America*, edited by W. L. Graf, *Centen. Spec.*, vol. 2, pp. 403–468, Geol. Soc. of Am., Boulder, Colo., 1987.

Baker, V. R., R. G. Strom, V. C. Gulick, J. S. Kargel, G. Komatsu, and V. S. Kale, Ancient oceans, ice sheets, and the hydrological cycle on Mars, *Nature*, *352*, 589–594, 1991.

Benn, D. I., and D. J. A. Evans, *Glaciers and Glaciation*, Oxford Univ. Press, New York, 1998.

Björnsson, H., Jökulhlaups in Iceland: Prediction, characteristics and simulation, *Ann. Glaciol.*, *16*, 95–106, 1992.

Carr, M. H., *Water on Mars*, 229 pp., Oxford Univ. Press, New York, 1996.
Chapman, M. G., C. C. Allen, M. T. Gudmundsson, V. C. Gulick, S. P. Jokobsson, B. K. Lucchitta, I. P. Skilling, and R. B. Waitt, Volcanism and ice interactions on Earth and Mars, in *Environmental Effects on Volcanic Eruptions: From Deep Oceans to Deep Space*, edited by T. Gregg and J. Zimbelman, pp. 39–73, Plenum, New York, 2000.
Clifford, S. M., A model for the hydrologic and climactic behavior of water on Mars, *J. Geophys. Res.*, *98*, 10,973–11,016, 1993.
Fishbaugh, K. E., J. W. Head, and S. Pratt, South polar chasmata: Analysis of MOLA data and evidence for basal melting and ponding in the Prometheus Basin, *Lunar Planet. Sci.* [CD-ROM], *XXXI*, abstract 1206, 2000.
Fishbaugh, K. E., and J. W. Head, Comparison of the north and south polar caps of Mars: New observations from MOLA data and discussion of some outstanding questions, *Icarus*, *153*, 1–17, 2001.
Ghatan, G. J., and J. W. Head, Candidate subglacial volcanoes in the south polar region of Mars, *Lunar Planet. Sci*. [CD-ROM], *XXXII*, abstract 1039, 2001.
Ghatan, G. J., and J. W. Head, Candidate subglacial volcanoes in the south polar regions of Mars: Morphology, morphometry, and eruption conditions, *J. Geophys. Res*., *107*, 10.1029/2001JE001519, in press, 2002.
Golombek, M. P., and N. T. Bridges, Erosion rates on Mars and implications for climate change: Constraints from the Pathfinder landing site, *J. Geophys. Res.*, *105*, 1841–1853, 2000.
Greeley, R., and J. E. Guest, Geologic map of the Eastern Equatorial Region of Mars, *U.S. Geol. Surv. Misc. Invest. Ser., Map I-1802-B*, 1987.
Grimm, R. E., and S. C. Solomon, Tectonic tests of proposed polar wander paths for Mars and the Moon, *Icarus*, *74*, 21–35, 1986.
Gudmundsson, M. T., F. Sigmundsson, and H. Bjornsson, Ice-volcano interaction of the 1996 Gjalp subglacial eruption, Vatnajokull, Iceland, *Nature*, *389*, 954–957, 1997.
Gulick, V. C., D. Tyler, C. P. McKay, and R. M. Haberle, Episodic ocean-induced CO_2 greenhouse on Mars: Implications for fluvial valley formation, *Icarus*, *130*, 68–86, 1997.
Haberle, R. M., Early Mars climate models, *J. Geophys. Res.*, *103*, 28,467–28,479, 1998.
Hartmann, W. K., and G. Neukum, Cratering chronology and the evolution of Mars, *Space Sci. Rev.*, *95*, 167–196, 2001.
Head, J. W., Extensive south polar cap in middle Mars history?: Tests using MOLA data, *Lunar Planet. Sci*. [CD-ROM], *XXXI*, abstract 1119, 2000a.
Head, J. W., Channels surrounding candidate ancient south polar deposits on Mars: Evidence for drainage of meltwater, *Lunar Planet. Sci*. [CD-ROM], *XXXI*, abstract 1121, 2000b.
Head, J. W., and G. J. Ghatan, Hesperian-aged ice-rich deposits near the south pole: Evidence for large-scale melting and drainage in the southern Noachis Terra region of Mars, *Lunar Planet. Sci*. [CD-ROM], *XXXII*, abstract 1062, 2001.
Head, J. W., and B. Hallet, Origin of sinuous ridges in the Dorsa Argentea Formation: Additional criteria for tests of the esker hypothesis, *Lunar Planet. Sci*. [CD-ROM], *XXXII*, abstract 1366, 2001a.
Head, J. W., and B. Hallet, Origin of sinuous ridges in the Dorsa Argentea Formation: New observations and tests of the esker hypothesis, *Lunar Planet. Sci*. [CD-ROM], *XXXII*, abstract 1373, 2001b.
Head, J. W., and S. Pratt, Extensive Hesperian-aged south polar ice cap on Mars: Evidence for massive melting and retreat, and lateral flow and ponding of meltwater, *J. Geophys. Res.*, *106*, 12,275–12,299, 2001a.
Head, J. W., and S. Pratt, Large Hesperian lake in Schmidt Valley near the south pole of Mars: Evidence for water input and drainage, *Lunar Planet. Sci*. [CD-ROM], *XXXII*, abstract 1159, 2001b.
Head, J. W., and L. Wilson, Mars: General environments and geological settings of magma/H_2O interactions, in *Volcano/Ice Interactions*, *Geol. Soc. Spec. Publ*., in press, 2002.
Head, J. W., III, M. A. Kreslavsky, and S. Pratt, Northern lowlands of Mars: Evidence for widespread volcanic flooding and tectonic deformation in the Hesperian Period, *J. Geophys. Res*., *107*(E1), 10.1029/2000JE001445, 2002.
Hoffman, N., White Mars: A new model for Mars' surface and atmosphere based on CO_2, *Icarus*, *146*, 326–342, 2000.
Ivanov, B. A., Mars/Moon cratering rate ratio estimates, *Space Sci. Rev.*, *95*, 89–106, 2001.
Jakosky, B. M., and R. J. Phillips, Mars' volatile and climate history, *Nature*, *412*, 237–244, 2001.
Kolb, E. J., and K. L. Tanaka, South polar region of Mars: Preliminary 1:3,000,000-scale mapping results, *Lunar Planet. Sci*. [CD-ROM], *XXXII*, abstract 2082, 2001.
Kreslavsky, M. I., and J. W. Head, The fate of outflow channel effluents in the Northern Lowlands of Mars: The Vastitas Borealis Formation, *Eos Trans. AGU*, *82*(20), Spring Meet. Suppl., P31A-03, 2001.
Longhi, J., Low-temperature phase relations in the CO_2-H_2O system with application to Mars, *Lunar Planet. Sci*. [CD-ROM], *XXXI*, abstract 1518, 2000.
Plaut, J., R. Kahn, E. Guiness, and R. Arvidson, Accumulation of sedimentary debris in the south polar region of Mars and implications for climate history, *Icarus*, *76*, 357–377, 1988.
Schultz, P. H., and A. Lutz, Polar wandering on Mars, *Icarus*, *73*, 91–141, 1988.
Scott, D. H., and K. L. Tanaka, Geologic map of the western hemisphere of Mars, *U.S. Geol. Survey Misc. Invest. Ser., Map I-1802-A*, 1986.
Strom, R. G., S. K. Croft, and N. G. Barlow, The Martian impact cratering record, in *Mars*, edited by H. H. Kieffer et al., pp. 383–423, Univ. of Ariz. Press, Tucson, 1992.
Tanaka, K. L., and D. Scott, Geologic map of the polar regions of Mars, *U.S. Geol. Survey Misc. Invest. Ser., Map I-1802-C*, 1987.
Tanaka, K. L., D. H. Scott, and R. Greeley, Global stratigraphy, in *Mars*, edited by H. H. Kieffer et al., pp. 345–382, Univ. of Ariz. Press, Tucson, 1992.
Thomas, P., S. Squyres, K. Herkenhoff, A. Howard, and B. Murray, Polar deposits of Mars, in *Mars*, edited by H. H. Kieffer et al., pp. 767–795, Univ. of Ariz. Press, Tucson, 1992.
Ward, W. R., Long-term orbital and spin dynamics of Mars, in *Mars*, edited by H. H. Kieffer et al., pp. 298–320, Univ. of Ariz. Press, Tucson, 1992.
Wilson, L., and J. W. Head, Heat transfer and melting in subglacial basaltic volcanic eruptions: Implications for volcanic deposit morphology and meltwater volumes, in *Volcano/Ice Interactions*, *Geol. Soc. Spec. Publ*., in press, 2002.
Zuber, M. T., et al., Internal structure and early thermal evolution of Mars from Mars Global Surveyor topography and gravity, *Science*, *287*, 1788–1793, 2000.

J. W. Head III, S. M. Milkovich, and S. Pratt, Department of Geological Sciences, Brown University, Box 1846, Providence, RI 02912, USA. (james_head_III@brown.edu)

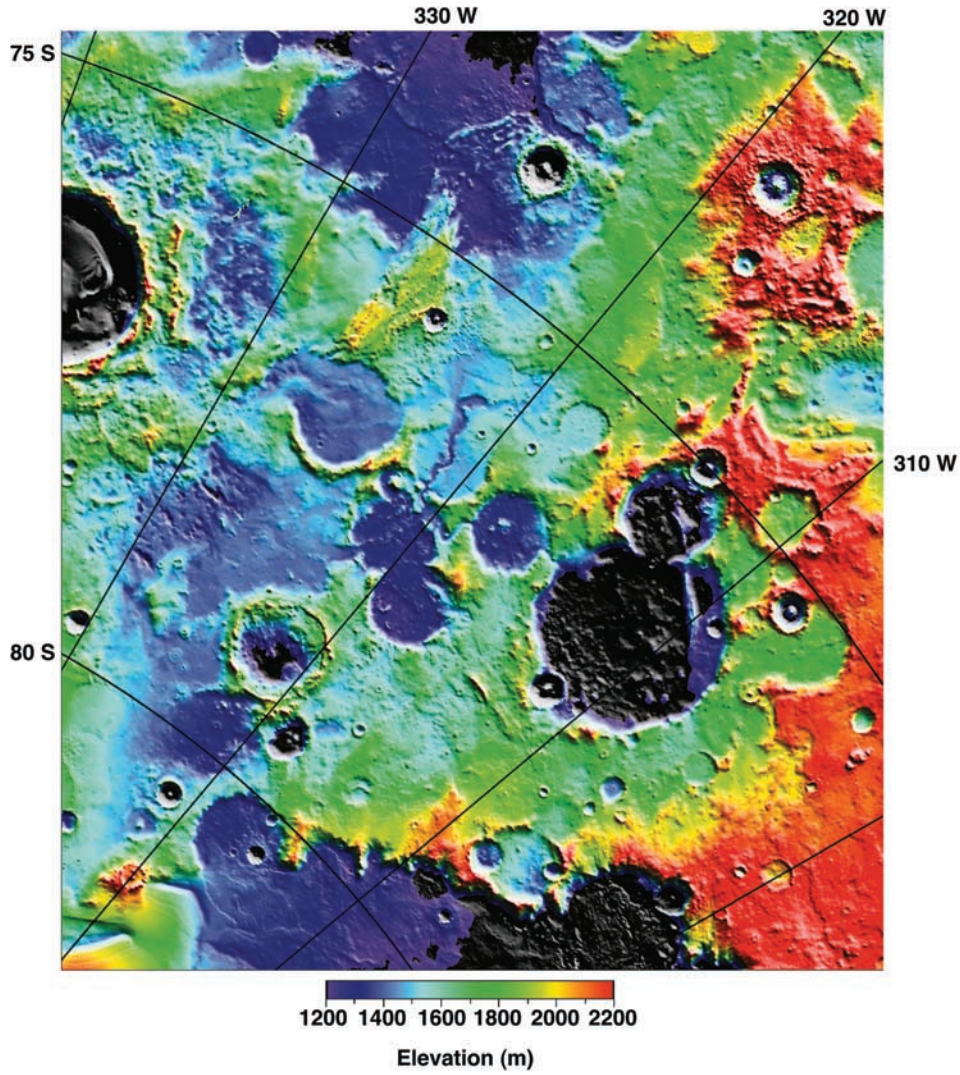

Figure 3. MOLA topography of the south polar region overlain on a topographic gradient map. The gradient map is generated from the same data sets used for topography and consists of directional point-to-point slopes encoded as gray scale. Illumination is from the northeast, and gray is flat, white is upslope, and black is downslope. Projection is stereographic.